Journal of Applied Mechanical Engineering
ISSN: 2168-9873

Qiang et al., J Appl Mech Eng 2018, 7:1
DOI: 10.4172/2168-9873.1000297

Research Article Open Access

Dynamic Characteristic of High Strength Ring Chain under Different Launch Parameters

Qiang Z*, Jun-Ming L, Yong-Feng L and Li-Ying L

Department of Mechanical Engineering, Liaoning Technical University, Fuxin 123000, P.R. China

Abstract

The aim of this study is to investigate the mechanical characteristics of the high strength ring chain under various launch parameters and the energy consumption law caused by this. Particularly, the contact dynamics simulation is implemented in Abaqus. In this study, the stress and strain contours of the high strength ring chain under the chain speeds of 1.85 m/min, 5.6 m/min, and 7.8 m/min and under the transportation loads of 2t, 3t, and 3.5t are obtained, plus their stress histories. Simulation results show that the corresponding steady stresses under distinct chain speeds are 748.2 MPa, 754.5 MPa, and 755.6 MPa, determining the optimal chain speed of 5.6m min^{-1}. After reaching the steady state, the maximum stresses under the loads of 2t, 3t, and 3.5t are 774.8 MPa, 758.1 MPa, and 747 MPa, respectively. Furthermore, the experimental results illustrate that the energy consumption caused by the friction among high strength ring chains under no-load operation occupies 23.8% of the resistance consumption. With the rise in loads, the total resistance consumption grows linearly. As a consequence, the research on the dynamic characteristics of the high strength ring chain is valuable for improving the working efficiency of the electromotor.

Keywords: High strength ring chain; Launch characteristics; Energy consumption analysis; Chain speed; Transportation load

Introduction

High strength ring chains are widely utilized as the hauling mechanism in transportation and lifting machineries, and because of the complicated loads generated by actual working conditions, high strength ring chains frequently generate fracture failure, which will affect the normal operation of devices adversely and even cause serious accidents. Therefore, the scholars worldwide are paying attention to this issue. Zhang et al. analysed the dynamic characteristics and impact damage of the scraper under various working conditions and chain speeds, obtaining corresponding mechanical properties [1]. He et al. investigated the contact characteristic between ring chains and sprocket wheel under different sorts of working condition (i.e., the full load launch, normal braking, and braking caused by the stuck ring chain) based on Abaqus, achieving the longitudinal dynamics model [2]. Wang, Yang, and Wang studied the abrasion characteristics of sprocket wheels in the scraper conveyer via the combination of the experiment and theory [3]. Mao, Zhang, and Shi designed the PID fuzzy controller of the chain tension and analysed the change laws of the chain tensions under different working conditions [4]. Zhang and Fu discussed the kinematic accuracy between plough chains and sprocket wheel with arbitrary distribution parameters and proposed a novel reliability-based robust design method [5]. Shi and Gao established the mechanical model of high strength ring chains and studied the effect of the inside width of ring chains on their mechanical properties through altering the loading frequency [6]. The above investigations can provide certain theoretical guidance for the prediction and analysis of the operating performance of high strength ring chains. However, the effect of launch parameters on the dynamic characteristics laws of ring chains is not illustrated clearly. To investigate the above issue systematically, the dynamic characteristics of ring chains under distinct launch parameters are executed in this study.

Establishment of Theoretical Model

For the majority of metal materials, they have both elastic and plastic deformations during the tensile process. Particularly, low-carbon steels are the typical representation of plastic materials, which has four obvious stages: the elastic stage, yield stage, hardening stage, and local necking stage. Generally, this sort of material is defined as the bilinearity or polyteny models to reflect the true stress-strain status. In addition, for the materials following Mises rule, the bilinear kinematic hardening model is utilized to cope with the minor strain and nonlinear problems of isotropic materials. For the majority of metal materials, the bilinear kinematic hardening model [7-9] is suitable for them. As discussed above, the bilinear kinematic plastic model is used in this study, as given by:

$$\sigma_y = \left[1 + \left(\frac{\dot{\varepsilon}}{C}\right)^{1/P}\right]\left(\sigma_0 + \beta E_P \varepsilon_P^{eff}\right) \quad (1)$$

where σ_y is the yield stress, σ_0 is the initial yield stress, $\dot{\varepsilon}$ is the strain ratio, C,P are the parameters of Cowper-Symonds strain ratio, ε_P^{eff} is the effective plastic strain, β is the hardening parameter, and E_P is the plastic hardening modulus.

The plastic hardening modulus is

$$E_P = \frac{E_{\tan} E}{E - E_{\tan}} \quad (2)$$

where E is the elastic modulus, and E_{tan} is the tangent modulus. 1 percent of the elastic modulus is selected as a reference to tangent modulus [10].

The bilinear model is used to simulate the constitutive relations of

***Corresponding author:** Qiang Z, Department of Mechanical Engineering, Liaoning Technical University, Fuxin 123000, China, Tel: +86 418 335 1111; E-mail: 415564476@qq.com

Received January 02, 2018; **Accepted** January 31, 2018; **Published** February 04, 2018

Citation: Qiang Z, Jun-Ming L, Yong-Feng L, Li-Ying L (2018) Dynamic Characteristic of High Strength Ring Chain under Different Launch Parameters. J Appl Mech Eng 7: 297. doi:10.4172/2168-9873.1000297

elastoplastic materials via two straight lines, which is considered the Hooke's law is satisfied in the elastic deformation stage. Take the elastic modulus as the slope, and take the tangent modulus as the slope after the plastic deformation occurs. The kinematic plastic material model is related to strain rate and can be considered losing efficacy whose model is a mixed model of isotropic, kinematic hardening or isotropic and kinematic hardening. The aforementioned hardening parameter β is used to measure the effect of kinematic hardening and isotropic hardening on the mechanical deformation process of the material, whose range is between 0 and 1. $\beta=0$ represents the material is only effected by kinematic hardening, and $\beta=1$ represents the material is only effected by isotropic hardening. For most metals, the material model is a bilinear kinematic hardening model.

PRO/E is used to establish the 3D model of ring chains, as shown in Figure 1. As shown in Figure 1, there are three intact ring chains and two semi-rings. For the convenience of applying loads and boundary conditions in Abaqus, let the ring chains at the both ends of the 3D model be semi-rings.

The chemical components of material and the corresponding mechanical properties are listed in Tables 1 and 2.

Launch characteristics under different chain speeds

To investigate the dynamic characteristics of ring chains under different chain speeds, three sorts of chain speed (i.e., 1.85 m/min, 5.6 m/min, and 7.8 m/min) are selected. In particular, the semi-ring 1 with the density of 7.3×10^{-4} t/mm^3 is used to represent the stuff with the mass of 3t in order to simulate the acceleration process. Through the simulation, the stresses and strains under different launch speeds are obtained, as shown in Figure 2.

As shown in Figure 2, the stress of element 4314 is the maximum, and the strain of element 4389 is the maximum. That is, the maximum stress and strain appear in the contact regions of ring chains. During the launch process, the contact regions bear most of impact, regardless of the effects from external factors. Particularly, the maximum stress and strain appear in the contact region of ring chains 3 and 4. As the ring chain 5 is applied on the velocity load, the ring chain 3 is pulled by the ring chain 4, and the stress concentration with an extremely high

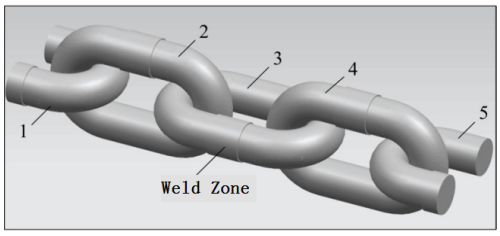

Figure 1: 3D model of ring chains.

Component	C	Mn	Si	S、P	Cr、Ni	Cu
Percentage (%)	0.07-0.24	1.40-1.80	0.17-0.37	≤0.025	≤0.30	≤0.25

Table 1: Chemical components and percentages of material.

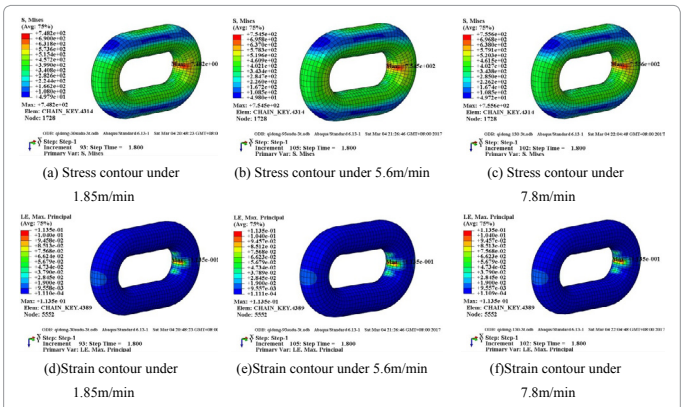

Figure 2: Contours of stress and strain under different launch speeds.

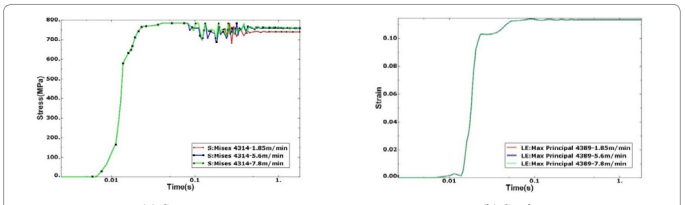

(a) Stress (b) Strain

Figure 3: The maximum stress and strain under different launch speeds.

value is generated because of the collision, showing that the ring chain stretched by others will generate the maximum stress.

The curves of the maximum stress and strain of elements 4314 and 4389 under different launch speeds are shown in Figure 3. For the convenience of analyzing the histories of the stress and strain, the time axis is set as the logarithmic coordinates. Figure 3a shows that the overall tendencies of the histories of the stress under different launch speeds are nearly consistent. From 0s to 0.07s, the stress keeps stable first, and then it increases dramatically. During this process, curves consist well with each other, showing that different launch speeds have slight effects on the stress within a short time. After that, stresses fluctuate swiftly for a period of 0.02s, and the differences of the amplitudes of stress oscillations are minor. Finally, fluctuations diminish gradually to constants. The above process illustrates that ring chains will strike each other repeatedly until a stable state is reached. When the time is 1s, ring chains reach a steady state, and the steady stresses under distinct chain speeds of 1.85 m/min, 5.6 m/min, and 7.8 m/min are 748.2 MPa, 754.5 MPa, and 755.6 MPa, showing that the larger launch speed is, the larger the steady stress will be. In terms of the full-load condition, the high launch speed will damage ring chains greatly, reducing its service life to certain extent.

Figure 3b shows that the histories of the strains under different launch speed overlap together. Before 0.014s, the strain increases slightly, and the fluctuation is extremely minor. During this period, the maximum strain is 0.003. When the time is 0.014s, the corresponding stress is 578.4 MPa, so the strain is the elastic strain during this period. After 0.014s, the strain climbs suddenly to 0.1mm at 0.022s, showing

Mechanical properties							Brinell hardness HB100
Tensilestres $s\sigma_b$/ MPa	Yield stress σ_s/MPa	Percentageelongationafter fracture σ_s/%	Percentage reduction of area Ψ/%	Impact energy A_k/ J	Elasticity modulus E/MPa	Poisson's ratio μ	
785	590	Greater or equal to 10	40	47	210000	0.28	Less or equal to 187

Table 2: Mechanical properties of materials.

that the plastic deformation is generated. In addition, the stress after 0.014s exceeds the yield stress, supporting the above point of view. From 0.022s to 0.031s, the strain rises smoothly, and during the same period, the increase of the stress is also slight. Afterwards, the strain goes up to 0.113, and the strain hardening is produced. Since the plastic deformation is permanent, the strain keeps stable despite of the decrease of the steady stress after 1s. This is the reason why the strain curves under distinct launch speeds overlap together.

Based on the above analysis, the launch speed affects the stress slightly from 0s to 0.07s, whereas it will have effects on the steady stress. With the rise in the launch speed, the steady stress will increase. Before 0.07s, the plastic deformation has already been generated, so the launch speed has slightly effects on the strain after 0.07s.

The launch process of ring chains is a kind of acceleration process, so the acceleration should be considered. The normal contact force of ring chains under different launch speeds is shown in Figure 4. Figure 4 shows that the normal contact force curves under different launch speeds basically overlap together from 0s to 0.1s. This indicates that during launch process, the elastic deformation and the contact gap of

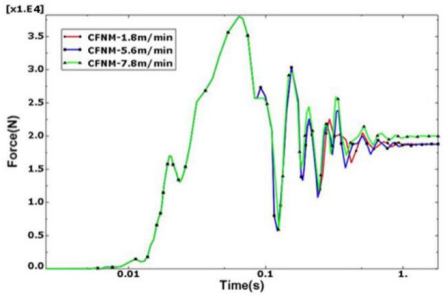

Figure 4: Normal contact force.

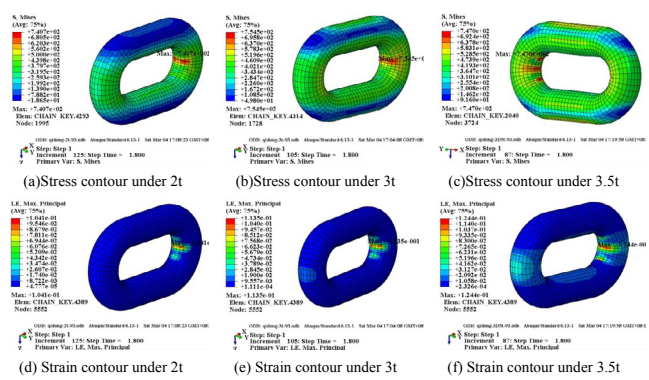

(a)Stress contour under 2t (b)Stress contour under 3t (c)Stress contour under 3.5t

(d) Strain contour under 2t (e) Strain contour under 3t (f) Strain contour under 3.5t

Figure 5: Contours of stress and strain under different loads.

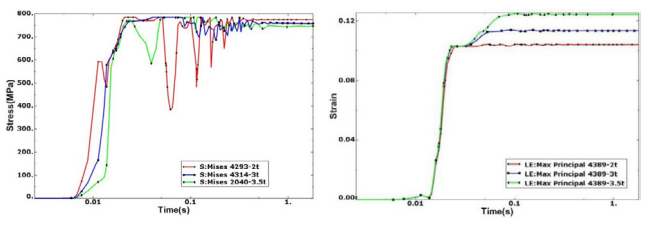

(a) Stress (b) Strain

Figure 6: The maximum stress and strain under different loads.

chain rings and initial speed have little influence on the contact force. The contact force of the chain suddenly reaches its peak value when the chain link is tight, after that, because of the impact, the normal resultant force of the chain fluctuates, and the amplitude of the fluctuation decreases gradually. When the time is 1s, the fluctuation amplitude is in 10 N, the system running smoothly; the contact force fluctuates slightly after 1s; and the system enters uniform running state after 1.5s. In the process of running shock, the contact force fluctuation is not regular between 0.1s and 0.25s, and the contact force at the launch speed of 7.8 m/min after 0.25s is significantly larger than the contact force of the other two speeds. After uniform motion, the contact force reached 20025 N at the launch speed of 7.8 m/min, however, the contact force at the launch speed of 1.85 m/min and 5.6 m/min was almost the same, which are 18771 N and 18785 N respectively. Thus, with the rise in launch speed, the normal contact force increases, and causes the chain having greater contact force, so that the chain wear increases, and the chain service life reduces; with the decrease in launch speed, the normal contact force is small, but the running efficiency is not high. Therefore, the starting speed of 5.6 m/min can take into account both running efficiency and wear resistance.

Launch characteristics under transportation load

In the real world, the external load is another factor affecting the dynamic characteristics of ring chains, and for some scraper conveyers, the full-load and overload conditions are very common to improve the production efficiency. In this study, three sorts of external loads (i.e., 2t, 3t, and 3.5t) are used to simulate the normal, specified, and overload working conditions. Particularly, the semi-ring 1 with the densities of 4.868×10^{-4}, 7.3×10^{-4}, and 8.519×10^{-4} t/mm^3 are used to represent these three external loads. The running velocity of the scraper conveyer is 5.6 m/min. In addition, the accelerative time is 1.5 s, and the even running time is 0.3 s. The obtained stresses and strains under different loads are shown in Figure 5.

Figures 5a-5c show that the maximum stresses under the loads of 2t and 3t are at the position of the middle area of the inside arc of ring chain 2. When the load of 3.5t is applied on ring chains, the position of the maximum stress is at the transition region between the inside arc and straight parts of ring chains, and the contact area is increased significantly. That is, when the weight of the transported stuff exceeds the rated load, the apparent stress concentration will appear, causing that the minor contact region is crushed and a larger contact area is produced among ring chains. In addition, because of the excessive load, the position of the maximum stress is changed from the stretched ring chain 3 to the ring chain 2, which is closer to the ring chain 1 with a mass of 3.5 t. Figures 5d-5f show that the maximum strain elements under different loads are all the element 4389, showing that different loads have no effects on the position of the maximum strain.

Figure 6a shows that when the ring chain bears a larger load, the lower steady stress will be generated. After reaching the steady state, the maximum stresses under the loads of 2t, 3t, and 3.5t are 774.8 MPa, 758.1 MPa, and 747 MPa, respectively. Figure 6b shows that with the rise in the load, the steady strain goes up. At 0.016s, the yield deformation is generated, so ring chains have already been failure when the maximum strain keeps stable. The larger strain will contribute to the larger contact area. Compared with loads, the contact area has significant effects on the stress [11,12]. This is the reason why with the rise in the load, there is a decrease in the stress.

The normal contact forces under different loads are shown in Figure 7. Figure 7 shows that the normal contact force curves under

different loads are similar to those under distinct launch speeds. The normal contact forces under different loads have three stages: the launch impact stage, swift fluctuation stage, and steady stage. However, the normal contact force of ring chains under the load of 3.5t rises significantly to 96475 N at 0.062s. After 1s, fluctuations under different loads remain stable. The steady contact force under the load of 2t is 17121 N, and the steady contact force under the load of 3t is 18785 N. By contrast, the steady contact force under the load of 3.5t is 59606 N, the highest value. Therefore, the normal contact force under the overload condition increases dramatically, which will damage ring chains seriously or fracture ring chains suddenly [13-16].

Experimental Detection and Analysis

To detect the dynamic characteristics of ring chains in real time, the ring chains in the actual scraper conveyer are used. Through the online test method, the detection of tension is fulfilled. During the detection, the force conditions of welded rings are observed, and the middle areas of two straight parts of the welded ring are milled as two plane domains, which can be used to install and protect welding strain-meters. In addition, some grooves are manufactured in the scraper to cover electric wires, and the data receiving device and power source are placed in two cavities, as shown in Figure 8. The experimental platform used in this study is shown in Figure 9.

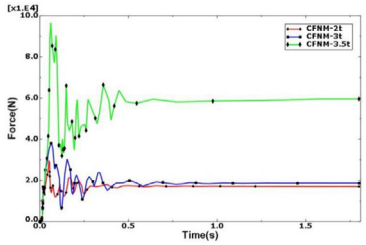

Figure 7: Normal contact force.

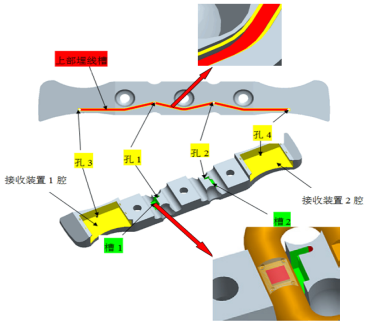

Figure 8: Installation instruction of instrument.

Figure 9: Experimental platform.

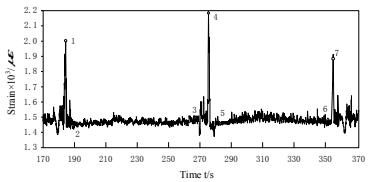

Figure 10: Strain history within a cycle period.

The welding strain-meters are connected with the receiving device via the electric wires in the wiring channel and holes. After launching the whole system, data are gathered and stored in the strain gathering module, and data are transported to the wireless gateway by means of the wireless transmission method. After system stops running, the data in the wireless strain gathering module are exported and analysed.

The experiment utilizes the quadratic fitting formula of the stress and load of ring chains given in Equation (3) to calculate the tension.

$$F_1 = -1.6e^{-5} \times ch_1^2 - 0.2657 \times ch_1 - 226.7 \quad (3)$$

Where ch_1 is the measured data (micro strain, με), and F_1 is the corresponding load, kN.

Discussion

Energy consumption of ring chains under no-load condition

The strain history within a cycle period under the normal operating condition is shown in Figure 10. The strains and tensions of special points shown in Figure 10 are listed in Table 2. In Table 2, numbers 1, 4, and 7 represent the maximum values of transient stresses when the scraper contacts with the sprocket wheel. Number 2 is the detected strain when the sensor is at the position of the lower point of the handpiece, whose tension is 112.73 kN. Number 3 is the detected strain when the sensor is at the position of the tail, whose tension is 121.99 kN. Obviously, the difference value is 9.26 kN when ring chains run between the lower points of the handpiece and tail. During the operation of the scraper conveyer, the tension of ring chains is caused by the running resistance, so the resistance of the scraper conveyer can be obtained in a special stage according to the computation of the tension. Therefore, the resistance from the lower point of the handpiece to that of the tail is 9.26 kN.

The computational formula of the friction between the scraper and chute is given by

$$F_f = \nu q_0 Lg \cdot \cos\theta \quad (4)$$

where ν is the friction coefficient between the scraper and chute and q_0 is the unit mass of ring chains,

L is the working length, g is the acceleration of gravity, and θ is the inclination angle.

$$W_z - \nu q_0 L^2 g \cdot \cos\theta = W_h \quad (5)$$

But

$$W_z = F_z L \quad (6)$$

where W_z is total energy consumption caused by the resistance, J, F_z is the total resistance, N, W_h is the energy consumption caused by the friction among ring chains, J.

When the scraper conveyer runs under the no-load condition, the resistance consumption is the main energy consumption. According to the experiment, it is obtained that the total energy consumption caused by the resistance from the lower point of the handpiece to that of the tail is 648200 J. Based on Equations (4) to (6), the energy consumption caused by the friction among ring chains is obtained, whose value is

Number	Strain/με	Tension/kN
1	2 497	279.75
2	1 889	142.73
3	1 977	151.99
4	2 669	292.97
5	1 458	115.10
6	1 487	124.68
7	1 880	210.76

Table 3: Strains and tensions of special points.

154280 J. The energy consumption caused by the friction among ring chains is 23.8% of the total energy consumption. In this study, the unit mass of ring chains is 25.2 kg/m, and the working length is 70m; the acceleration of gravity is 10 N/kg.

Energy consumption of ring chains under load condition

When the external load of 3t is applied on the scraper, the strains and dynamic tensions of detected ring chains are listed in Table 3. Through the experiment, the total resistance caused by the ring chains running from the bottom of the handpiece to the bottom of the tail is obtained. In particular, the total energy consumption caused by the resistance is 858200 J. With the rise in external load, the total energy consumption caused by the resistance increases 210000 J.

The relationship between the total energy consumption caused by the resistance and load is

$$W_h = 7 \times 10^3 F + 6.482 \times 10^5 \quad (7)$$

where F is the external load, t.

Conclusions

(1) The steady stresses under distinct chain speeds of 1.85 m/min, 5.6 m/min, and 7.8 m/min are 748.2 MPa, 754.5 MPa and 755.6 MPa, determining the optimal chain speed of 5.6 m/min.

(2) The steady stresses under different loads of 2t, 3t, and 3.5t are 774.8 MPa, 758.1 MPa and 747 MPa, respectively. The normal contact force of ring chains increases swiftly under the overload launch condition, which will damage ring chains greatly and probably generate the fracture failure.

(3) The online test method for the ring chain tension is proposed, and experimental analysis is carried out on the experimental platform. The experimental result shows that the load is proportional to the total resistance consumption.

Acknowledgements

Thanks for the funds as following:Ministry of Education PhD Fund: Study on cracking rate of mining ring chain induced by temperature stress corrosion coupling (20132121120011); Key Laboratory of structural analysis of industrial equipment open fund (Dalian University of Technology): Research on Reliability and Life Design of Chain Transmission System of Scraper Conveyor (GZ1402); State Key Laboratory of mechanical transmission open fund (Chongqing University): The theory and key technology of high efficiency transmission of scraper conveyor chain (SKLMT-KFKT-201515); Liaoning Natural Science Fund Project (20161324): Study on multi information fusion recognition of coal rock interface based on physical and cutting characteristics

References

1. Zhang Q, Wang H, Guo T, Fu Y (2016) Dynamic characteristics and impact damage of mining scrapers under different working conditions and chain speeds. J Vibration and Shock 35: 51-58.
2. He B, Sun Y, Nei R, Li G (2012) Dynamic behavior analysis on the ring chain transmission system of an armoured face conveyor. J Mech Eng 17: 50-56.
3. Wang S, Yang Z, Wang X (2014) Wear of driving sprocket for scraper convoy and mechanical behaviors at meshing progress. J China Coal Society 1: 166-171.
4. Mao J, Zhang D, Shi J (2008) Simulation research of tension automatic control system of scraper conveyor. J System Simulation 16: 4474-4476.
5. Zhang Q, Fu Y (2013) Reliability-based robust design for kinematic accuracy of the plow plane chain mesh with arbitrary distribution parameters base on nsga-algorithm. J China Coal Society 38: 505-511.
6. Shi L, Gao yu (2005) Experimental study of chain fatigue life. J Taiyuan University of Technology 3: 270-272.
7. Xue H, Liu L, Yang Z, Shiyuan Z, Tong K (2011) Effect of low temperature and strain rate on impact property of mining chain. J Xi'an University of Science and Technology 3: 343-346.
8. Zhang Q, Xu M (2014) Study on fatigue life of plow bit under different planning parameters. Strength of Materials 46: 262-269.
9. Wang H, Zhang Q (2017) Dynamic tension test and intelligent coordinated control system of a heavy scraper conveyor. IET Science, Measurement & Technology.
10. He T, Yang J, Jin X (2007) ANSYS10.0/LS-DYNA nonlinear finite element analysis example tutorial. China Machine Press, P.R. China.
11. Dang X, Ma X (2017) Influence of asperity collision on contact stress and strain. Tribology 1: 11-18.
12. Wang M, Li Z, Ma X (2016) Influence of sphere contact area on stress of t-shape bolt in fastener. Railway Engineering 12: 102-104.
13. Zhang Q, Wang H, Mao J, Zhang D, Yuan Z (2015) Self-powered tension testing system for scraper conveyor based on piezoelectric vibration energy harvested. Chinese J Sensors and Actuators 28: 1335-1340.
14. Zhang Q, Wang H, Fu Y, Gong J (2015) Mechanical property and fatigue life prediction of sprocketin scraper conveyor. J Mechanical Strength 37: 328-336.
15. Luo Q (1997) Analysis of fatigue of strength round link chain for mine uses. J China Coal Society 22: 95-99.
16. Zhao Y (2015) The dynamic research on hoisting mechanism of crane based on virtual prototype technology. Shanghai University of Engineering Science, China.